Controlling the Cadence and Admittance of a Functional Electrical Stimulation Cycle

Christian A. Cousin, Courtney A. Rouse, Victor H. Duenas, and Warren E. Dixon

***Abstract*— For an individual suffering from a neurological condition, such as spinal cord injury, traumatic brain injury, or stroke, motorized functional electrical stimulation (FES) cycling is a rehabilitation strategy, which offers numerous health benefits. Motorized FES cycling is an example of physical human–robot interaction in which both systems must be controlled; the human is actuated by applying neuromuscular electrical stimulation to the large leg muscle groups, and the cycle is actuated through its onboard electric motor. While the rider is stimulated using a robust sliding-mode controller, the cycle utilizes an admittance controller to preserve rider safety. The admittance controller is shown to be passive with respect to the rider, and the cadence controller is shown to be globally exponentially stable through a Lyapunov-like switched systems stability analysis. Experiments are conducted on three able-bodied participants and four participants with neurological conditions (NCs) to demonstrate the efficacy of the developed controller and investigate the effect of manipulating individual admittance parameters. Results demonstrate an average admittance cadence error of -0.06 ± 1.47 RPM for able-bodied participants and -0.02 ± 0.93 RPM for participants with NCs.**

***Index Terms*— Functional electrical stimulation (FES), rehabilitation robot, Lyapunov, admittance, passivity.**

I. Introduction

WITHIN the United States, there are millions of people suffering from debilitating neurological conditions (NCs) such as spinal cord injury (SCI), traumatic brain injury, Parkinson's disease (PD), and stroke, among others. Stroke alone affects 800,000 Americans annually and leaves millions of people permanently disabled [1]. Because NCs can cause damage to the brain, spinal cord, or nerves, they can manifest themselves in incredibly complex ways, oftentimes compromising a person's ability to properly utilize and accurately control their neuromuscular system. Consequently, people may suffer from negative secondary side-effects such as diabetes, obesity, and muscle atrophy, etc. resulting from sedentary lifestyles. To improve the overall quality of life and activities of daily living of these affected individuals, multiple efforts are being made in the field of rehabilitation, namely hybrid exoskeletons, which combine functional electrical stimulation (FES) and rehabilitation robots [2], resulting in physical human-robot interaction.

FES is the application of an electric field across the motor neurons of a muscle to induce an artificial, involuntary contraction to perform a functional movement. Numerous benefits of FES have been reported throughout literature such as increased muscle mass, increase bone mineral density, and improved cardiovascular parameters, among others [3], [4].

Rehabilitation robots have also been reported to improve sensory perception and motor function [5]–[7]. Rehabilitation robots should be able to accommodate every unique individual instead of holding them all to the same standard (i.e., the same cadence or torque objective) [8]. Admittance control, established by Hogan [9], provides an intuitive method for rehabilitation robots to safely interact with humans without unduly forcing them to adhere to predefined trajectories [10]. Admittance control allows force feedback to modify desired trajectories, and based on the parameters selected, can modify it to various degrees designed assist or resist a person [11].

Hybrid exoskeletons attempt to blend the advantages of FES and rehabilitation robotics while mitigating the drawbacks of each. However, hybrid exoskeletons are inherently challenging to implement, particularly when applied to people whose neuromuscular systems are severely compromised [10]. Additionally, the dynamics of both muscle activation and robotic systems are nonlinear and uncertain [12]. An example of a hybrid exoskeleton is a motorized FES cycle; it includes the application of FES to a person's leg muscles to cooperatively pedal a recumbent cycle along with an electric motor attached to the cycle [12]. The benefits of performing FES cycling combine the benefits of rehabilitation robots and FES; however, they may be reduced compared to volitional cycling due to the early onset of fatigue caused by the external (and not physiologically optimized) activation of motor units within muscle and other obstacles to rehabilitation [13]–[15]. Furthermore, because the sensation from FES can be uncomfortable [16] and the benefits from FES are reported to culminate over long time periods (cf. [16], [17]), improved FES cycles (and

Manuscript received November 21, 2018; revised February 8, 2019; accepted April 15, 2019. Date of publication May 3, 2019; date of current version June 6, 2019. This work was supported in part by the NSF under Award DGE-1842473, Award DGE-1315138, and Award 1762829. *(Corresponding author: Christian A. Cousin.)*

C. A. Cousin, C. A. Rouse, and W. E. Dixon are with the Department of Mechanical and Aerospace Engineering, University of Florida, Gainesville, FL 32611 USA (e-mail: ccousin@ufl.edu; courtneyarouse@ufl.edu; wdixon@ufl.edu).

V. H. Duenas is with the Department of Mechanical and Aerospace Engineering, Syracuse University, Syracuse, NY 13244 USA (e-mail: vhduenas@syr.edu).

This paper has supplementary downloadable material available at http://ieeexplore.ieee.org, provided by the author.

Digital Object Identifier 10.1109/TNSRE.2019.2914579

controllers) are needed to accelerate the benefits and reduce the discomforts. Recently, FES cycling gained significant attention at the 2016 Cybathlon in Zürich, Switzerland where an FES cycling race was one of six competitive events designed for people with physical disabilities. Of the eleven teams to complete the race, all used open-loop methods or rider-controlled stimulation parameters [18], where the efficiency advantages of implanted electrodes were demonstrated by the winning team.

Other FES cycling studies have been produced which similarly modulate the FES input (and/or the current actuating the cycle's motor) using open-loop methods [19], or closed-loop methods such as linear [20] or nonlinear control techniques (e.g., fuzzy logic, sliding mode) [21]. Few of these results, however, provide a rigorous stability analysis, required to illustrate rider safety. Moreover, because pedaling a cycle involves the cooperation of multiple muscle groups, FES cycling is a state-dependent switched system, which requires a switched systems analysis and design methods [22].

As in other hybrid exoskeletons (cf. [11], [23], [24]), to improve user comfort and safety, the motorized FES cycle in this paper utilizes admittance control, rather than other control methods such as cadence [12], [25] or cadence and torque [26] control. While the listed results in [12], [25], [26] do provide a rigorous switched systems stability analysis, they do not include admittance control of FES cycling. With admittance control of motorized FES cycles, the cadence trajectory is allowed to deviate based on force-feedback from the rider to better accommodate for unique cases and rider capabilities. By selectively modifying the admittance parameters (i.e., the injected inertia and damping), the admittance controller is capable of emulating a cadence controller (by increasing the inertia and damping) or admitting to the rider significantly (by decreasing the inertia and damping). By appropriately selecting the admittance parameters, the cycle can be made increasingly stiff or compliant by activating the cycle's motor accordingly. Hence, if the rider is unable to pedal at the desired speed, the cycle can assist the rider in maintaining a desired cadence to a degree dictated by the selected admittance parameters. In other words, admittance control is more concerned about the dynamic behavior of the system instead of explicit position or torque tracking [9].

While admittance control has been extensively used on rehabilitation robots, to the authors' knowledge it has only been implemented on an FES cycle in the authors' previous works, such as in [27]–[29], which this work is predicated upon. Compared to our previous results, this work includes a complete stability analysis for both the admittance and cadence controllers; results on four participants with NCs and three able-bodied participants, compared to results on a single able-bodied participant (cf. [27], [28]); and an in-depth analysis of the results based on each participant's NC.

In this paper, a combined admittance/cadence controller is developed for implementation on an FES cycle to simultaneously pedal the FES cycle and stimulate the rider's muscles. The admittance controller is implemented on the cycle's motor and the robust sliding-mode cadence controller is applied to the rider's muscle groups. Closed-loop control allows the electrical stimulation to be adjusted online to account for the nonphysiological recruitment of muscle fibers, and over time, fatigue. Furthermore, the FES delivered to the rider's muscle groups is saturated for comfort, and due to the admittance controller, the cycle responds appropriately by slowing down if the delivered stimulation is insufficient to produce the desired torque at the desired cadence. While the cycle's motor is active for all time, the rider's muscles are activated only when they can efficiently contribute torque about the crank. Heuristically, the cycle strikes a balance between rider safety (which addresses muscle/joint spasticity by allowing the rider to deviate from the desired cadence) and capability. Using a Lyapunov-like switched systems stability analysis, the cadence controller is proven to be globally exponentially stable and the admittance controller is proven to be passive with respect to the rider.

Experiments were conducted on four participants with various NCs (i.e., spina bifida, spinal cord injury, post-stroke hemiparesis, and Parkinson's disease) and three able-bodied participants to demonstrate feasibility and desired performance metrics. Admittance parameters were varied across all protocols and the admittance controller achieved an average admittance cadence error of -0.06 ± 1.47 RPM for able bodied participants and -0.02 ± 0.93 RPM for participants with NCs. Experimental results validate the controllers which hold promise for a novel cycling experience to promote rehabilitation while ensuring safety and comfort.

II. Dynamics

A. Cycle-Rider System

The nonlinear, uncertain cycle-rider dynamics can be modeled as[1] [12]

$$M(q)\ddot{q} + V(q,\dot{q})\dot{q} + G(q) + P(q,\dot{q}) + b\dot{q} + d(t) = \underbrace{B_m(q,\dot{q})u_m(t)}_{\tau_m(q,\dot{q},t)} + \underbrace{B_e u_e(t)}_{\tau_r(t)}, \quad (1)$$

where $q : \mathbb{R}_{\geq 0} \to \mathcal{Q}$, $\dot{q} : \mathbb{R}_{\geq 0} \to \mathbb{R}$, and $\ddot{q} : \mathbb{R}_{\geq 0} \to \mathbb{R}$ denote the measurable crank angle, calculable angular velocity (cadence), and unknown acceleration, respectively; and $\mathcal{Q} \subseteq \mathbb{R}$ denotes the set of achievable crank angles. The torque contribution from the rider's leg muscles is denoted by $\tau_m : \mathcal{Q} \times \mathbb{R} \times \mathbb{R}_{\geq 0} \to \mathbb{R}$, and the torque contribution from the cycle's electric motor is denoted by $\tau_r : \mathbb{R}_{\geq 0} \to \mathbb{R}$. The inertial, centripetal-Coriolis, and gravitational effects of the combined cycle-rider system are denoted by $M : \mathcal{Q} \to \mathbb{R}$, $V : \mathcal{Q} \times \mathbb{R} \to \mathbb{R}$, and $G : \mathcal{Q} \to \mathbb{R}$, respectively. The torques from the rider's passive viscoelastic tissue and the cycle's friction are denoted by $P : \mathcal{Q} \times \mathbb{R} \to \mathbb{R}$ and $b : \mathbb{R}_{>0} \to \mathbb{R}$, respectively. System disturbances are denoted by $d : \mathbb{R}_{\geq 0} \to \mathbb{R}$. The subsequently designed muscle control input (i.e., electrical stimulation) is denoted by $u_m : \mathbb{R}_{\geq 0} \to \mathbb{R}$, the known motor control constant relating the motor's input current to output torque is denoted by $B_e \in \mathbb{R}_{>0}$, and the subsequently designed motor control current is denoted by

[1]For notational brevity, all explicit dependence on time, t, within the states $q(t)$, $\dot{q}(t)$, $\ddot{q}(t)$ is suppressed.

$u_e : \mathbb{R}_{\geq 0} \to \mathbb{R}$. The unknown, nonlinear lumped muscle control effectiveness $B_m : \mathcal{Q} \times \mathbb{R} \to \mathbb{R}_{>0}$ is defined as

$$B_m(q, \dot{q}) \triangleq \sum_{m \in \mathcal{M}} b_m(q, \dot{q}) k_m \sigma_m(q), \tag{2}$$

where the set $\mathcal{M}$ includes the right and left quadriceps femoris, gluteal, and hamstring muscle groups, respectively, and accounts for the summed torque contribution arising from the muscle groups of the legs when stimulated. Furthermore, the unknown, nonlinear individual muscle control effectiveness mapping input stimulation to output torque is denoted by $b_m : \mathcal{Q} \times \mathbb{R} \to \mathbb{R}_{>0}$, and the constant muscle control gains are denoted by $k_m \in \mathbb{R}_{>0}$. The piecewise right-continuous switching signals for the activation of the individual muscle groups are denoted by $\sigma_m : Q \to \{0, 1\}$ and defined as [12]

$$\sigma_m(q) \triangleq \begin{cases} 1 & q \in \mathcal{Q}_m \\ 0 & q \notin \mathcal{Q}_m \end{cases}, \tag{3}$$

$\forall m \in \mathcal{M}$, where $\mathcal{Q}_m \subset \mathcal{Q}$ denotes the region in which muscle group m is stimulated. The regions are defined as

$$\mathcal{Q}_m \triangleq \{q \in \mathcal{Q} \mid T_m(q) > \varepsilon_m\}, \tag{4}$$

$\forall m \in \mathcal{M}$, where $T_m : \mathcal{Q} \to \mathbb{R}$ denotes the torque transfer ratio of each muscle group about the cycle's crank. The selectable torque transfer threshold is denoted by $\varepsilon_m \in \left(0, \max\left(T_m(q)\right)\right]$ and dictates the angles at which each muscle group is stimulated based on its respective kinematic effectiveness. Because the torque transfer ratios are dependent on each rider's leg geometry, they are calculated independently for each rider and based on the result in [12]. The torque transfer threshold is selected such that backpedaling is prevented, stimulation is only applied when each muscle group can positively contribute to the motion of the crank (i.e., $\varepsilon_m > 0$, $\forall m \in \mathcal{M}$), and muscle fatigue is delayed by only stimulating muscles in kinematically efficient regions (i.e., $\tau_m(q) > \varepsilon_m$, $\forall m \in \mathcal{M}$). The union of all muscle stimulation regions establishes the combined FES region of the crank cycle, defined as $\mathcal{Q}_M \triangleq \bigcup_{m \in \mathcal{M}} \mathcal{Q}_m$, and the kinematic deadzone (KDZ) region as the remainder $\mathcal{Q}_K \triangleq \mathcal{Q} \backslash \mathcal{Q}_M$. By discretely switching between muscle groups to control continuous dynamics, a state-dependent switched system is created. Although the parameters in (1) capture the torques affecting the dynamics of the combined cycle-rider system, the exact value of these parameters are unknown for each rider. However, the subsequently designed controllers only require known bounds on the aforementioned parameters. Specifically, the following properties [12] are provided for the switched system in (1)[2]:

Property 1: The inertia parameter is upper- and lower-bounded by $c_m \leq M \leq c_M$, where c_m, $c_M \in \mathbb{R}_{>0}$ are known constants.

Property 2: The centripetal-Coriolis parameter is upper-bounded by $|V| \leq c_V |\dot{q}|$, where $c_V \in \mathbb{R}_{>0}$ is a known constant.

[2]For notational brevity, all functional dependencies are hereafter suppressed unless required for clarity of exposition.

Property 3: The torque generated by gravity is upper-bounded by $|G| \leq c_G$, where $c_G \in \mathbb{R}_{>0}$ is a known constant.

Property 4: The torque generated by the rider's viscoelastic tissues is upper-bounded by $|P| \leq c_{P1} + c_{P2} |\dot{q}|$, where c_{P1}, $c_{P2} \in \mathbb{R}_{>0}$ are known constants.

Property 5: The torque generated by the cycle's friction is upper-bounded by $b \leq c_b$, where $c_b \in \mathbb{R}_{>0}$ is a known constant.

Property 6: The torques generated by system disturbances are upper-bounded by $|d| \leq c_d$, where $c_d \in \mathbb{R}_{>0}$ is a known constant.

Property 7: The system is skew-symmetric by the relation $\dot{M} - 2V = 0$.

Property 8: The individual muscle control effectiveness, b_m, is subject to nonlinear activation dynamics and a muscle fiber recruitment curve (commonly represented by sigmoidal function) [30], [31]. However, when $q \in \mathcal{Q}_M$, the lumped, unknown muscle control effectiveness mapping the FES input to the output muscle force, and hence, torque about the cycle's crank, is bounded by $B_{\underline{m}} \leq B_m \leq B_{\overline{m}}$, where $B_{\underline{m}}$, $B_{\overline{m}} \in \mathbb{R}_{>0}$ are known constants [32].

III. Control Development

The following section includes the development of an admittance controller for the cycle's motor and cadence controller for the rider's muscles. The admittance controller is designed to be passive with respect to the rider to ensure safety and used to indirectly track a desired torque to assist the rider in maintaining cycle cadence. The cadence controller is used to directly regulate cycle cadence in the FES regions by rejecting the torque from the admittance controller.

A. Admittance Controller

While the rider's muscles regulate cadence in the FES regions (i.e., while $q \in \mathcal{Q}_M$), the cycle's controller is designed such that it will resist the rider if the cadence is too high (i.e., $\dot{q} > \dot{q}_d$) or assist the rider if the cadence is too low (i.e., $\dot{q} < \dot{q}_d$) in both the FES and KDZ regions (i.e., $q \in \mathcal{Q}$) , where $\dot{q}_d : \mathbb{R}_{\geq 0} \to \mathbb{R}$ denotes the desired cadence. The assistance modality is vital because the rider's muscles only contribute torque about the crank in the FES regions; therefore when the rider's muscles are inactive in the KDZ regions, the cycle is expected to decelerate. Admittance control is commonly used as a method of indirect torque tracking, and therefore, employs an interaction torque error, quantified by $e_\tau : \mathbb{R}_{\geq 0} \to \mathbb{R}$, and defined as

$$e_\tau \triangleq \tau_{int} - \tau_d, \tag{5}$$

where the desired interaction torque is denoted by $\tau_d : \mathbb{R}_{\geq 0} \to \mathbb{R}$, and $\tau_{int} : \mathbb{R}_{\geq 0} \to \mathbb{R}$ denotes the measurable bounded interaction torque between the cycle and rider (i.e., $\tau_{int} \in \mathcal{L}_\infty$) [33], [34]. By subsequently implementing an admittance filter, the interaction torque error can be transformed into an admitted trajectory, which can be tracked using an inner-loop position controller. The admittance filter is designed as

$$e_\tau \triangleq M_d \ddot{q}_a + B_d \dot{q}_a, \tag{6}$$

where $q_a,\ \dot{q}_a,\ \ddot{q}_a : \mathbb{R}_{\geq 0} \to \mathbb{R}$ denote the admitted position, velocity, and acceleration, respectively; and $M_d,\ B_d \in \mathbb{R}_{>0}$ denote the desired inertia and damping, respectively. To ensure boundedness of the admitted trajectory, the parameters in (6) are selected such that the transfer function of (6) is passive [35, Lemma 6.4]. After the admitted trajectory is generated by (6), an inner-loop position controller is designed to track the admittance error system, quantified by $\xi : \mathbb{R}_{\geq 0} \to \mathbb{R}$ and $\psi : \mathbb{R}_{\geq 0} \to \mathbb{R}$, defined as

$$\xi \triangleq q_a + q_d - q, \tag{7}$$

$$\psi \triangleq \dot{\xi} + \beta \xi, \tag{8}$$

where $q_d : \mathbb{R}_{\geq 0} \to \mathbb{R}$ denotes the desired position, designed to be sufficiently smooth (i.e., $q_d,\ \dot{q}_d,\ \ddot{q}_d \in \mathcal{L}_\infty$). Hence, if the position controller can regulate the errors in (7) and (8), the controller will preserve the admitted dynamics of the filter in (6) and accomplish its indirect torque tracking objective. The open-loop admittance error system is generated by taking the time derivative of (8), multiplying by M, adding and subtracting ξ, and substituting (1), (7), and (8) to yield

$$M\dot{\psi} = \chi_1 - B_e u_e - \tau_m - V\psi - \xi, \tag{9}$$

where the lumped auxiliary signal $\chi_1 : \mathcal{Q} \times \mathbb{R} \times \mathbb{R}_{\geq 0} \to \mathbb{R}$ is defined as $\chi_1 \triangleq M\left(\ddot{q}_a + \ddot{q}_d + \beta\psi - \beta^2\xi\right) + V\left(\dot{q}_d + \beta\xi + \dot{q}_a\right) + G + P + b\left(\dot{q}_a + \dot{q}_d - \psi + \beta\xi\right) + d + \xi$ and is bounded by Properties 1-6 as $|\chi_1| \leq c_1 + c_2||\phi|| + c_3||\phi||^2$, where $c_1,\ c_2,\ c_3 \in \mathbb{R}_{>0}$ are known constants, $\|\cdot\|$ denotes the standard Euclidean norm, and the error vectors $\phi \in \mathbb{R}^4$ and $\zeta \in \mathbb{R}^2$ are defined as $\phi \triangleq \left[\zeta^T,\ \dot{q}_a,\ \ddot{q}_a\right]^T$ and $\zeta \triangleq [\xi,\ \psi]^T$, respectively. Based on (9) and the subsequent stability analysis, the admittance controller is designed as

$$u_e \triangleq \frac{1}{B_e}\left[k_1\psi + \left(k_2 + k_3\|\phi\| + k_4\|\phi\|^2\right)\operatorname{sgn}(\psi)\right], \tag{10}$$

where $\operatorname{sgn}(\cdot)$ denotes the signum function, included to provide robustness to the uncertainty in χ_1, and $k_i \in \mathbb{R}_{>0}\ \forall i = 1,\ 2,\ 3,\ 4$ denote constant control gains. Substituting (10) into (9) yields the closed-loop admittance error system

$$M\dot{\psi} = \chi_1 - \tau_m - V\psi - \xi - \left[k_1\psi + \left(k_2 + k_3\|\phi\| + k_4\|\phi\|^2\right)\operatorname{sgn}(\psi)\right]. \tag{11}$$

B. Cadence Controller

While the cycle is assigned to regulate the admitted error system throughout the entire crank cycle (i.e., $q \in \mathcal{Q}$), the cycle's cadence is regulated using the rider's muscles in the FES regions (i.e., $q \in \mathcal{Q}_M$). The cadence tracking objective is quantified by $e : \mathbb{R}_{\geq 0} \to \mathbb{R}$ and $r : \mathbb{R}_{\geq 0} \to \mathbb{R}$, each defined as

$$e \triangleq q_d - q, \tag{12}$$

$$r \triangleq \dot{e} + \alpha e, \tag{13}$$

where $\alpha \in \mathbb{R}_{>0}$ denotes a constant control gain. The open-loop cadence error system is obtained by taking the derivative of (13), multiplying by M, adding and subtracting e, and substituting (1), (12), and (13) to yield

$$M\dot{r} = \chi_2 - B_m u_m - B_e u_e - Vr - e, \tag{14}$$

where the lumped auxiliary signal $\chi_2 : \mathcal{Q} \times \mathbb{R} \times \mathbb{R}_{\geq 0} \to \mathbb{R}$ is defined as $\chi_2 \triangleq M\left(\ddot{q}_d + \alpha r - \alpha^2 e\right) + V\left(\dot{q}_d + \alpha e\right) + G + P + b\left(\dot{q}_d - r + \alpha e\right) + d + e$ and bounded by Properties 1-6 as $|\chi_2| \leq c_4 + c_5\|z\| + c_6\|z\|^2$, where $c_4,\ c_5\ c_6 \in \mathbb{R}_{>0}$ are known constants, and the error vector $z \in \mathbb{R}^2$ is defined as $z \triangleq [e,\ r]^T$. Based on (14) and the subsequent stability analysis, the cadence controller is designed as

$$u_m = \frac{1}{\underline{B_m}}\Big[k_5 r + \Big(k_6 + k_7\|z\| + k_8\|z\|^2 + k_9|u_e|\Big)\operatorname{sgn}(r)\Big], \tag{15}$$

where $\operatorname{sgn}(\cdot)$ is included to provide robustness to the uncertainty in χ_2, $k_i \in \mathbb{R}_{>0}\ \forall i = 5,\ 6,\ \ldots, 9$ denote constant control gains, $\underline{B_m}$ is introduced in Property 8, and u_e is included to overcome the torque supplied by the motor. Substituting (15) into (14) yields the closed-loop cadence error system

$$M\dot{r} = \chi_2 - B_e u_e - Vr - e - \frac{B_m}{\underline{B_m}}\Big[k_5 r + \Big(k_6 + k_7\|z\| + k_8\|z\|^2 + k_9|u_e|\Big)\operatorname{sgn}(r)\Big]. \tag{16}$$

IV. Stability Analysis

For the following theorems, let $V_1 : \mathbb{R}^2 \to \mathbb{R}$ denote a positive definite storage function defined as

$$V_1 \triangleq \frac{1}{2}M\psi^2 + \frac{1}{2}\xi^2, \tag{17}$$

which satisfies the following inequalities: $\underline{\gamma}\|\zeta\|^2 \leq V_1 \leq \overline{\gamma}\|\zeta\|^2$, where $\underline{\gamma},\ \overline{\gamma} \in \mathbb{R}_{>0}$ are known constants defined as $\underline{\gamma} \triangleq \frac{1}{2}\min(c_m,\ 1)$, and $\overline{\gamma} \triangleq \frac{1}{2}\max(c_M,\ 1)$. Let $V_2 : \mathbb{R}^2 \to \mathbb{R}$ denote a positive definite Lyapunov function candidate defined as

$$V_2 \triangleq \frac{1}{2}Mr^2 + \frac{1}{2}e^2, \tag{18}$$

which satisfies the following inequalities: $\underline{\gamma}\|z\|^2 \leq V_2 \leq \overline{\gamma}\|z\|^2$.

Theorem 1: Given the closed-loop admittance error system in (11) and the admittance relation in (6), the admittance controller in (10) is passive from input $|\tau_m|$ to output $|\psi|$, provided the constant gain conditions are satisfied: $k_2 \geq c_1,\ k_3 \geq c_2,\ k_4 \geq c_3$. Furthermore, when in isolation (i.e., decoupled from the rider and $\tau_m = 0$) the admittance error system is globally exponentially stable in the sense that

$$\|\zeta(t)\| \leq \sqrt{\frac{\overline{\gamma}}{\underline{\gamma}}}\|\zeta(t_0)\|\exp\left[-\frac{\delta}{2\overline{\gamma}}(t - t_0)\right], \tag{19}$$

$\forall t \in [t_0,\ \infty)$, *where* $\delta \triangleq min(k_1,\ \beta)$.

Proof: Let $\zeta(t)$ for $t \in [t_0,\ \infty)$ be a Filippov solution to the differential inclusion $\dot{\zeta} \in K[h_1](\zeta)$, where $K[\cdot]$ is defined as in [36], and where $h_1 : \mathbb{R}^2 \to \mathbb{R}^2$ is defined as $h_1 \triangleq \left[\dot{\xi}\ \ \dot{\psi}\right]^T$. Because of the discontinuity in the motor controller

in (10), the time derivative of V_1 exists almost everywhere (a.e.) (i.e., for almost all $t \in [t_0, \infty)$), and $\dot{V}_1(\zeta) \overset{\text{a.e.}}{\in} \dot{\tilde{V}}_1(\zeta)$, where $\dot{\tilde{V}}_1$ is the generalized time derivative of V_1 along the Filippov trajectories of $\dot{\zeta} = h_1(\zeta)$ [37]. Using the calculus of $K[\cdot]$ from [37], and substituting (8) and (9) into $\dot{\tilde{V}}_1$ yields

$$\dot{\tilde{V}}_1 \subseteq -\beta\xi^2 + \psi\chi_1 + \left(\frac{1}{2}\dot{M} - V\right)\psi^2 - k_1\psi^2 - \psi\tau_m - \left(k_2 + k_3||\phi|| + k_4||\phi||^2\right) K[\text{sgn}(\psi)]\psi, \quad (20)$$

where $K\left[\text{sgn}(\cdot)\right] = \text{SGN}(\cdot)$ such that $\text{SGN}(\cdot) = \{1\}$ if $(\cdot) > 0$, $[-1, 1]$ if $(\cdot) = 0$, and $\{-1\}$ if $(\cdot) < 0$. Hence, by Properties 1-7, and since $\dot{V}_1(\zeta) \overset{\text{a.e.}}{\in} \dot{\tilde{V}}_1(\zeta)$, (20) can bounded above as

$$\dot{V}_1 \overset{\text{a.e.}}{\leq} |\psi|\,|\tau_m| - \beta\xi^2 - k_1\psi^2 - |\psi|\left(\lambda_1 + \lambda_2\|\phi\| + \lambda_3\|\phi\|^2\right), \quad (21)$$

where $\lambda_1,\ \lambda_2,\ \lambda_3 \in \mathbb{R}$ are defined as $\lambda_1 \triangleq k_2 - c_1$, $\lambda_2 \triangleq k_3 - c_2$, $\lambda_3 \triangleq k_4 - c_3$. Provided the gain conditions listed above are satisfied, $\lambda_1,\ \lambda_2,\ \lambda_3 \geq 0$, thus (21) can be upper bounded as

$$\dot{V}_1 \overset{\text{a.e.}}{\leq} |\psi|\,|\tau_m| - \delta\|\zeta\|^2, \quad (22)$$

where δ was defined previously. Hence, by [35, Definition 6.3] the robot system is output strictly passive with input $|\tau_m|$, output $|\psi|$, and storage function V_1. When the robot acts in isolation (i.e., the human is decoupled from the robot), $\tau_m = 0$, and (22) can be rewritten using (17) as

$$\dot{V}_1 \overset{\text{a.e.}}{\leq} -\frac{\delta}{\bar{\gamma}}V_1. \quad (23)$$

Hence, the storage function qualifies as a radially unbounded positive definite Lyapunov function per the zero-state observability condition [35, Definition 6.5] and results in global exponential stability when $\tau_m = 0$. Using (17) with (23) provides the result in (19). Because the interaction torque is bounded, from the perspective of the robot, the physically applied rider torque is similarly bounded. Hence, from the closed-loop error system in (11), the admittance relation in (6), and the passivity result in (22), the robot admittance controller in (10) is bounded. ■

Remark 1: The rider's stimulation-elicited torque contribution is defined as $\tau_m \triangleq B_m u_m$, however, τ_m can be redefined to include the riders volitional torque contribution, $\tau_{vol} : \mathbb{R}_{\geq 0} \to \mathbb{R}$, as $\tau_m \triangleq B_m u_m + \tau_{vol}$ [38] and the conclusion of Theorem 1 still holds. Hence, if the rider volitionally contributes to pedaling the cycle in addition to the stimulation, the admittance controller is still passive.

For the following theorem, let $t_n^M \in \mathbb{R}_{\geq 0}$ denote the time the crank enters $\mathcal{Q}_M$ of cycle n, and $t_n^K \in \mathbb{R}_{\geq 0}$ as the time the crank enters $\mathcal{Q}_K$ (i.e., exits $\mathcal{Q}_M$) of cycle n.

Theorem 2: Given the closed-loop cadence error system in (16), for $q \in \mathcal{Q}_M$, global exponential tracking is guaranteed in the sense that

$$\|z(t)\| \leq \sqrt{\frac{\bar{\gamma}}{\underline{\gamma}}}\left\|z(t_n^M)\right\| \exp\left[-\frac{\rho}{2\bar{\gamma}}(t - t_n^M)\right], \quad (24)$$

$\forall t \in \left[t_n^M, t_n^K\right)$, $\forall n$, *where* $\underline{\gamma}$, $\bar{\gamma} \in \mathbb{R}_{>0}$ *maintain their definitions from above, and* $\rho \triangleq \min(k_5, \alpha)$, *provided the constant gain conditions are satisfied:* $k_6 \geq c_4$, $k_7 \geq c_5$, $k_8 \geq c_6$, $k_9 \geq B_e$.

Proof: Similar to the proof of Theorem 1, let $z(t)$ for $t \in [t_0, \infty)$ be a Filippov solution to the differential inclusion $\dot{z} \in K[h_2](z)$ and let $h_2 : \mathbb{R}^2 \to \mathbb{R}^2$ be defined as $h_2 \triangleq \left[\dot{e}\ \dot{r}\right]^T$. Using Property 7, and substituting (13) and (14) into $\dot{\tilde{V}}_2(z)$ yields

$$\dot{\tilde{V}}_2 \subseteq -\alpha e^2 - \frac{K[B_m]}{B_{\underline{m}}}k_5 r^2 - rB_e K[u_e] - \frac{K[B_m]}{B_{\underline{m}}}\left(k_6 + k_7\|z\| + k_8\|z\|^2 + k_9 K[|u_e|]\right)K[\text{sgn}(r)]r + r\chi_2, \quad (25)$$

where $K\left[|\text{sgn}(\cdot)|\right] = |\text{SGN}(\cdot)|$ such that $|\text{SGN}(\cdot)| = \{1\}$ if $(\cdot) \neq 0$, $[0, 1]$ if $(\cdot) = 0$. Note $K[B_m]$ can be lower bounded by $K\left[B_{\underline{m}}\right]$ by Property 8, and in the FES regions, $B_{\underline{m}}$ is continuous; therefore $K\left[B_{\underline{m}}\right]$ can be replaced with $B_{\underline{m}}$. This fact, along with Properties 1-6, and the fact that $\dot{V}_2(z) \overset{\text{a.e.}}{\in} \dot{\tilde{V}}_2(z)$, allows (25) to be evaluated in the FES regions and upper bounded as

$$\dot{V}_2 \overset{\text{a.e.}}{\leq} -\alpha e^2 - k_5 r^2 - |r|\left(\lambda_4 + \lambda_5\|z\| + \lambda_6\|z\|^2 + \lambda_7 \sup\left(K[|u_e|]\right)\right), \quad (26)$$

where $\lambda_i \in \mathbb{R}_{>0}\ \forall i = 4,\ 5,\ \ldots, 7$ are defined as $\lambda_4 \triangleq k_6 - c_4$, $\lambda_5 \triangleq k_7 - c_5$, $\lambda_6 \triangleq k_8 - c_6$, and $\lambda_7 \triangleq k_9 - B_e$. Provided the aforementioned gain conditions are satisfied, $\lambda_i \geq 0\ \forall i$; thus, (26) can be upper bounded using (18) as

$$\dot{V}_2 \overset{\text{a.e.}}{\leq} -\frac{\rho}{\bar{\gamma}}V_2, \quad (27)$$

where ρ was introduced in (24). Based on (18) and (27) the result in (24) can be obtained. From the result of Theorem 1, and from the closed-loop error systems, the cadence controller in (15) is bounded. ■

Remark 2: Redefining the rider's torque contribution as $\tau_m \triangleq B_m u_m + \tau_{vol}$ no longer guarantees exponential tracking; instead, by assuming the rider is contributing positive torque about the crank, it guarantees the actual cadence will be at least the desired cadence (i.e., $\dot{q} \geq \dot{q}_d$).

V. Experiments

A. Experimental Testbed

The experimental testbed was constructed by outfitting an existing recumbent tricycle (TerraTrike Rover) with sensors and actuators. An SRM Science Road Powermeter was substituted for the original bike crank to measure torque and a US Digital H1 encoder was attached to the crank via spur gears to measure position and cadence. A 250 W motor (Unite Motor Co. Ltd. MY1016Z2) was coupled to the drive chain and actuated using a current-controlled Advanced Motion Controls[3]

[3]ADVANCED Motion Controls supported the development of this testbed by providing discounts on their branded items.

TABLE I
PARTICIPANT DEMOGRAPHICS

Participant	Age	Sex	Condition	Active in FES	Active in PT/OT*	Physical Aid†	TSI‡
P1	25	M	None	- -	- -	- -	- -
P2	25	M	None	- -	- -	- -	- -
P3	24	F	None	- -	- -	- -	- -
P4	25	M	Spina Bifida (L5-S1), Arnold Chiari Malformation	Y	Y	AFO, Wheelchair	25yr
P5	28	F	Spinal Cord Injury (T8-T9)	N	N	Wheelchair	12yr
P6	50	F	Hemorrhagic Stroke	Y	Y	Wheelchair	4yr
P7	64	M	Parkinson's Disease	N	Y	- -	19yr

*PT/OT: Physical therapy/ occupational therapy
†AFO: ankle-foot orthosis
‡TSI: Time since injury

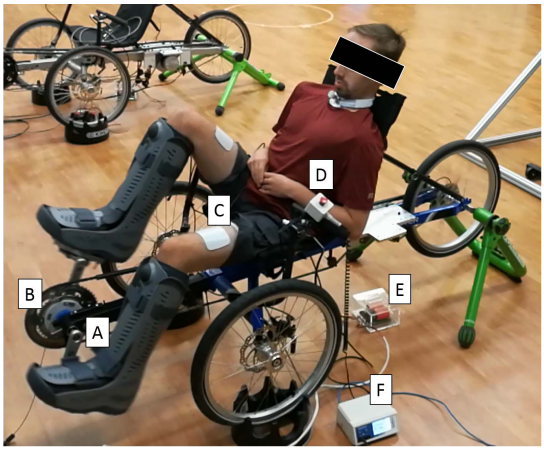

Fig. 1. Motorized FES cycle: (A) Encoder. (B) Power meter. (C) Electrodes. (D) E-Stop. (E) Filter card. (F) Stimulator.

(AMC) PS300W24 power supply and AMC AB25A100 motor driver. An AMC FC15030 filter card was added in-line with the motor to reduce electrical noise. The rider was coupled to the cycle with Orthotic boots (Össur Rebound Air Tall) attached at the pedals to maintain sagittal alignment of the legs and constrain the ankles. The cycle was offset from the ground using a trainer and riser rings. The encoder, powermeter, and motor were interfaced with a desktop computer running MATLAB/Simulink/Quarc through a Quanser Q-PIDe data acquisition board at 500 Hz. A current-controlled Hasomed Rehastim stimulator delivered symmetric, biphasic, and rectangular pulses via bipolar self-adhesive PALS®[4] electrodes to the rider's quadriceps, hamstrings, and gluteal muscle groups at respective amplitudes of 90 mA, 80 mA, and 70 mA at a frequency of 60 Hz. An emergency stop switch was attached to the cycle's handle to allow the rider to immediately halt the experiment if needed [12]. A rider seated on the motorized FES cycle is depicted in Figure 1.

B. Experimental Methods

Four experimental protocols (i.e., Protocols A, B, C, and D) were conducted on three able-bodied participants and four participants with NCs, whose demographics are listed in Table I. Each protocol had a duration of two minutes with the first twenty seconds consisting of a smooth motor-only ramp to the desired cadence of 50 RPM. Subsequently, the controllers in (10) and (15) were activated for the remaining duration of the experiment. Across all protocols, the desired inertia parameter was held constant at $M_d = 2\ \frac{Nm \cdot s^2}{rad}$ and the damping parameter was selected to be a low $\left(1\ \frac{Nm \cdot s}{rad}\right)$, medium $\left(2.5\ \frac{Nm \cdot s}{rad}\right)$, or high value $\left(5\ \frac{Nm \cdot s}{rad}\right)$ (i.e., Protocols A, B, and C, respectively) to investigate the effects of modifying the parameter. For Protocols A, B, and C, all participants were asked to remain passive, contribute no volitional torque, and were blind to the desired trajectory for the duration of the experiment. An additional protocol was conducted with the medium damping parameter, but with added volition (i.e., Protocol D) where the participants were shown a running plot of the measured and desired cadences. For Participants 1-3, the interaction torque was selected as $\tau_d = 0.5$ Nm for Protocols A-C, and as $\tau_d = 2.0$ Nm for Protocol D. For Participants 4-7, the interaction torque was selected as $\tau_d = 0.0$ Nm for Protocols A-D, unless otherwise noted.

The stimulation input in (15) was saturated based on individual participant comfort and was determined prior to experimentation. The experimental protocols were approved by the Institutional Review Board at the University of Florida. Participants are referred to by the letter "P" followed by their participant number. Unique trials are referred to by the participant number followed by the protocol letter; for example, Participant 3 Protocol B is referred to as P3B.

C. Results and Discussion

To estimate the power generated by the rider, an average passive torque reading, denoted by $\tau_p : \mathbb{R}_{\geq 0} \to \mathbb{R}$, was collected during each trial for 4.8 seconds prior to controller activation (i.e., approximately four crank cycles at 50 RPM) to provide a baseline estimate for the passive torque required to actuate the combined rider-cycle system at the desired cadence. Subsequently, an average estimate of the power generated by the rider, denoted by $P : \mathbb{R}_{\geq 0} \to \mathbb{R}$, was obtained through the relation, $P = \text{mean}\,(\dot{q})\,(\text{mean}\,(\tau_{int}) - \tau_p)$. Results from the seven participants are provided in Table II, with details on the average and standard deviation of the measured

[4]Surface electrodes for this study were provided compliments of Axelgaard Manufacturing Co., Ltd.

TABLE II
EXPERIMENTAL RESULTS, REPORTED AS AVERAGE±STANDARD DEVIATION

Participant	Protocol	$\dot{q}$ (RPM)	$\dot{q}_a$ (RPM)	$\dot{\xi}$ (RPM)	τ_{int} (Nm)*	τ_p (Nm)$^{\triangle}$	P (W)	u_e (A)	u_m (μs)$^{\square}$
P1	A	47.19±1.95	-2.95±1.48	-0.14±1.53	0.15±0.57	-0.61±0.51	3.80±2.84	2.19±1.00	134.51±26.98
	B	48.48±1.64	-1.63±0.91	-0.12±1.56	0.04±0.59	-0.63±0.50	3.44±3.00	2.33±1.01	110.99±29.60
	C	49.23±1.57	-0.90±0.65	-0.14±1.55	0.00±0.65	-0.57±0.49	2.93±3.38	2.16±1.04	83.19±20.87
	D	49.88±1.68	-0.26±0.76	-0.15±1.84	1.87±0.84	-0.58±0.51	12.84±4.39	0.24±1.24	43.48±4.58
P2	A	48.38±2.05	-1.62±1.38	-0.01±1.65	0.29±0.63	-0.58±0.59	4.47±3.20	1.94±1.13	103.65±20.26
	B	48.53±1.93	-1.48±1.16	-0.02±1.63	0.07±0.73	-0.69±0.58	3.91±3.72	2.27±1.15	106.79±25.18
	C	48.74±1.55	-1.30±0.57	-0.04±1.47	-0.21±0.57	-0.74±0.55	2.70±2.91	2.57±1.03	88.45±25.14
	D	49.54±1.70	-0.52±0.67	-0.06±1.72	1.79±0.84	-0.66±0.67	12.79±4.36	0.34±1.23	48.63±7.07
P3	A	49.19±2.20	-0.83±1.87	-0.03±1.26	0.38±0.45	-0.43±0.33	4.26±2.34	1.93±0.87	90.61±11.52
	B	49.22±1.76	-0.79±1.14	-0.01±1.36	0.28±0.51	-0.38±0.31	3.47±2.65	2.02±1.10	87.14±16.57
	C	49.25±1.41	-0.78±0.68	-0.04±1.24	0.06±0.50	-0.45±0.31	2.72±2.59	2.14±0.91	72.39±17.36
	D	50.01±1.44	-0.05±0.55	-0.07±1.43	1.93±0.60	-0.27±0.30	11.60±3.16	0.37±1.02	32.23±3.56
Mean	**A**	**48.25±2.06**	**-1.80±1.59**	**-0.06±1.48**	**0.20±0.55**	**- -**	**4.17±2.81**	**2.02±1.00**	**109.59±20.58**
Mean	**B**	**48.74±1.78**	**-1.30±1.07**	**-0.05±1.52**	**0.13±0.61**	**- -**	**3.60±3.15**	**2.20±1.08**	**101.64±24.39**
Mean	**C**	**49.07±1.65**	**-0.99±0.86**	**-0.07±1.42**	**-0.05±0.57**	**- -**	**2.78±2.95**	**2.29±0.99**	**81.34±21.36**
P4	A	46.23±1.20	-3.79±0.92	-0.02±0.87	-0.41±0.22	-0.46±0.25	0.22±1.08	2.56±0.60	60.38±10.69
	B	48.46±1.00	-1.56±0.41	-0.03±0.96	-0.42±0.23	-0.47±0.27	0.25±1.19	2.67±0.65	55.64±12.90
	C	49.29±0.97	-0.72±0.23	-0.02±0.96	-0.39±0.23	-0.46±0.27	0.37±1.22	2.55±0.65	46.10±11.95
	D†	49.53±1.61	-0.51±0.86	-0.05±1.46	0.82±0.72	-0.47±0.26	6.75±3.75	1.31±1.02	45.62±6.70
P5	A	44.42±1.27	-5.60±1.12	-0.03±0.73	-0.61±0.18	-0.56±0.22	-0.20±0.84	2.44±0.50	356.76±182.84
	B	47.86±0.87	-2.17±0.40	-0.03±0.81	-0.58±0.19	-0.53±0.27	-0.26±0.96	2.39±0.55	233.13±162.57
	C	48.95±0.86	-1.04±0.20	0.00±0.85	-0.56±0.20	-0.51±0.27	-0.24±1.03	2.46±0.58	172.88±109.94
	D$^{||}$	- -	- -	- -	- -	- -	- -	- -	- -
P6	A	45.52±1.05	-4.51±0.89	-0.03±0.64	-0.49±0.16	-0.61±0.15	0.56±0.77	2.22±0.44	56.01±9.90
	B	47.60±0.92	-2.42±0.50	-0.03±0.83	-0.65±0.26	-0.54±0.22	-0.54±1.29	2.38±0.57	53.31±11.58
	C	48.98±0.84	-1.04±0.30	-0.02±0.80	-0.55±0.26	-0.45±0.17	-0.52±1.38	2.30±0.56	42.51±12.72
	D	49.53±1.12	-0.48±0.65	-0.02±0.97	-0.13±0.42	-0.15±0.27	0.1±2.18	1.82±0.68	29.27±6.09
P7	A‡	44.80±1.82	-5.25±1.37	-0.05±1.47	1.39±0.92	-0.13±0.21	7.19±4.31	0.20±1.03	86.87±12.58
	B‡	48.29±1.30	-1.75±0.74	-0.04±1.16	0.51±0.55	-0.31±0.15	4.16±2.79	1.16±0.81	84.06±16.33
	C	50.04±0.87	0.01±0.26	-0.02±0.86	0.00±0.31	-0.19±0.18	1.06±1.62	1.66±0.60	29.38±3.45
	D†	49.94±1.23	-0.09±0.44	-0.03±1.27	0.94±0.67	-0.19±0.21	5.97±3.51	0.72±0.88	30.67±3.40
Mean	**A**	**45.24±1.36**	**-4.78±1.09**	**-0.03±0.98**	**-0.03±0.48**	**- -**	**1.94±2.29**	**1.85±0.68**	**140.00±91.92**
Mean	**B**	**48.05±1.03**	**-1.97±0.53**	**-0.03±0.95**	**-0.28±0.33**	**- -**	**0.90±1.71**	**2.15±0.65**	**106.53±82.15**
Mean	**C**	**49.31±0.90**	**-0.55±0.25**	**-0.01±0.86**	**-0.37±0.25**	**- -**	**0.16±2.03**	**2.24±0.59**	**72.71±55.68**

*A positive interaction torque signifies the participant was able to overcome the torque deficit required to passively actuate their legs.
†Due to volitional ability, the desired interaction torque was lowered to $\tau_d = 1.0$ Nm.
‡Due to minor volitional contributions by P7, the interaction torque was increased to $\tau_d = 2.0$ Nm for Protocol A and $\tau_d = 1.0$ for Protocol B.
||This run was not performed because the participant was unable to contribute volitionally.
△The average passive torque is participant-dependent and was not averaged.
□The average and standard deviation of the applied stimulation was calculated using the maximum stimulation delivered to each muscle group for each FES region.

cadence, admitted cadence, admitted cadence error, measured interaction torque, measured passive torque, and generated power. The controller gains in (8), (10), (13), and (15) were selected as $k_1 = 6$, $k_2 = k_3 = k_4 = 0.01$, $k_5 \in [2,\ 4]$, $k_6 = k_7 = k_8 = 0.1$, $k_9 = 0.5$, $\alpha \in [1,\ 8]$, $\beta \in [0.8,\ 1.2]$ across all trials. The aforementioned gain conditions are sufficient to achieve stability based on conservative bounds on the uncertain parameters in the dynamics. Therefore, the sufficient gain conditions provide guidelines for the initial gain selection and the gains can be subsequently adjusted to achieve desirable performance. Although the listed gains were adjusted using an empirical-based method, the gains could have been adjusted using more methodical approaches. For example, the nonlinear system in [39] was linearized at several operating points and a linear controller was designed for each point, and the gains were chosen by interpolating, or scheduling the linear controllers. In [40], a neural network is used to adjust the gains of a PID controller. In [41] a genetic algorithm was used to adjust the gains after an initial guess. The authors in [42] provide an extensive discussion on the use of extremum seeking for tuning the gains of a PID controller. Additionally, in [43], the tuning of a PID controller for robot manipulators is discussed.

By varying the damping parameter in the admittance filter in (6), various behaviors can be obtained from the cycle without changing any other aspect of the control system. For example, a high damping parameter results in a stiffer, less compliant cycle that admits less to any rider-applied torque. Based on Table II, it can be seen that increasing the damping parameter results in better cadence tracking, but less torque production (e.g., compare P1A to P1C). This is due to less position error accumulating in the cadence controller (because

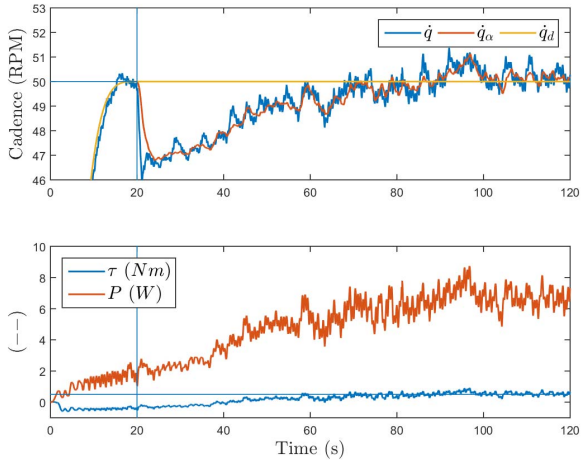

Fig. 2. P3B: (Top) Measured ($\dot{q}$), admitted ($\dot{q}_a$), and desired cadences ($\dot{q}_d$); (Bottom) Measured torque (τ) and estimated power (P) produced by the rider. Vertical lines represent time of controller activation, horizontal lines represent desired values (for cadence and torque).

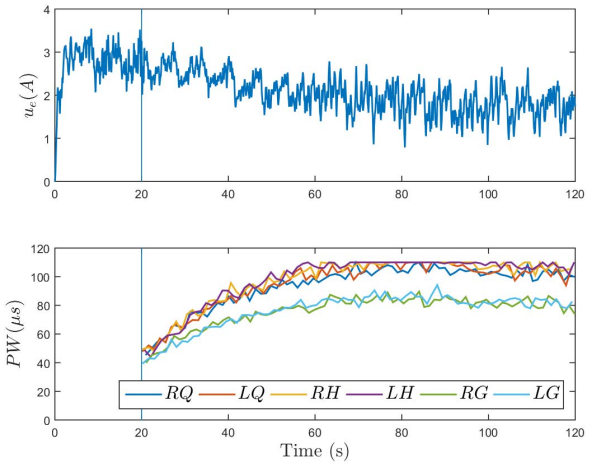

Fig. 3. P3B: (Top) Control effort sent to motor (Bottom) Control effort sent to rider's right (R) and left (L) quadriceps (Q), hamstring (H), and gluteal (G), respectively. Stimulation was saturated at 110 μs for rider comfort.

the cycle admits less) and consequently, less stimulation and torque production over time. With a low damping parameter, the admitted trajectory (i.e., $\dot{q}_a$) is allowed to deviate more than with a high damping parameter (see Column 4 of Table II), and the position error accumulates more quickly, resulting in more stimulation and torque production. Regardless of the cadence tracking error, the admittance tracking error is small in comparison across all experiments and participants (see Column 5 of Table II), indicating the motor is able to emulate the dynamics dictated by the admittance filter in (5) and (6). As the rider is stimulated, their muscles produce an interaction torque about the crank (i.e., τ_{int}); if this torque is greater than the passive amount it takes to actuate their body (i.e., τ_p), the interaction torque will be positive. Any torque reading greater than τ_p is assumed to be the result of torque generated by the rider's muscles and the difference is multiplied by the measured cadence to get an estimate of the power generated by the rider.

To facilitate the following discussion, let $\dot{q}_\alpha : \mathbb{R}_{\geq 0} \to \mathbb{R}$ denote the *admitted cadence trajectory*, defined as $\dot{q}_\alpha \triangleq \dot{q}_d + \dot{q}_a$, in contrast to the *admitted trajectory* denoted by $\dot{q}_a$. Note that although admittance error system is passive with respect to the rider, the admittance controller tracks the admitted trajectory closely. The cadence error system is proven to be exponentially stable, and Figure 2[5] indicates that when the participant is below their saturation level of 110 μs, the measured cadence converges to the desired cadence. Figure 2 also illustrates P3B's torque production, which over time, reaches the desired value of 0.5 Nm and demonstrates indirect regulation of the torque tracking error e_τ. Upon reaching the desired torque, the stimulation begins to plateau, as shown in Figure 3.[6] When the desired torque is reached, the admitted cadence trajectory begins to align with the desired cadence trajectory, and the participant is able to achieve the desired cadence at the desired torque. An estimate of the power produced by P3B is displayed in Figure 2 alongside the torque produced. Taken together, Figures 2 and 3 indicate that as the participant's stimulation increases, her muscles produce stronger contractions. Correspondingly, she is able to offset a portion of the torque required by the motor because it needs to assist the rider less. This results in a decrease of the amount of current required to actuate the motor. Of note, by offsetting a portion of the motor current needed to actuate the cycle with FES, smaller motors can be utilized, resulting in lighter, less powerful, and less expensive FES cycles.

To highlight the performance of a participant with a NC, Figures 4 and 5 display the tracking results and control inputs for P4B, respectively. As shown in Table II, the admittance tracking error is small as in the other participants, demonstrating convergence of the admittance error system. However, unlike P3, P4 had a low tolerance to the electrical stimulation. Consequently, only low levels of torques were able to be evoked, and the desired interaction torque was reduced from 0.5 Nm to 0 Nm. Note that due to the passive torque required to actuate P4's legs (i.e., approximately 0.46 Nm), an interaction torque of 0 Nm would still require P4's leg muscle to produce an average torque of 0.46 Nm. As illustrated in Figure 4, P4 was unable to achieve the desired torque production; hence, the admitted cadence trajectory consistently lagged the desired cadence trajectory. However, P4 was able to produce a small amount of torque, as indicated in Figure 4. As the experiment progresses, the participant begins to show signs of fatigue and his torque begins to decline (at approximately $t = 55$ s). As mentioned in [30], the early onset of fatigue remains an outstanding challenge in the use of FES. Despite the participant not achieving the desired cadence or desired torque (due to stimulation limitations, or actuator saturation), the admittance controller was still able to achieve stable operation and ensure participant safety and comfort. As seen in Table II, the average cadence achieved is directly related to the selected damping parameter, regardless of stimulation saturation.

[5]For visual clarity, a one-second moving average filter was applied to all cadence/torque plots.

[6]For visual clarity, a half-second moving average filter was applied to the motor current input. The stimulation input is represented as the maximum stimulation for each FES region at the corresponding time.

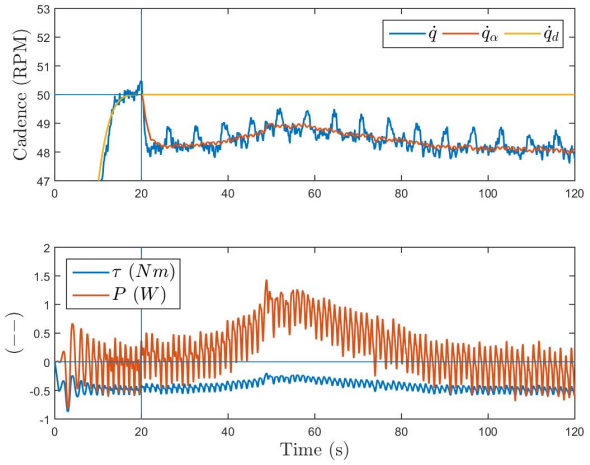

Fig. 4. P4B: (Top) Measured ($\dot{q}$), admitted ($\dot{q}_a$), and desired cadences ($\dot{q}_d$); (Bottom) Measured torque (τ) and estimated power (P) produced by the rider.

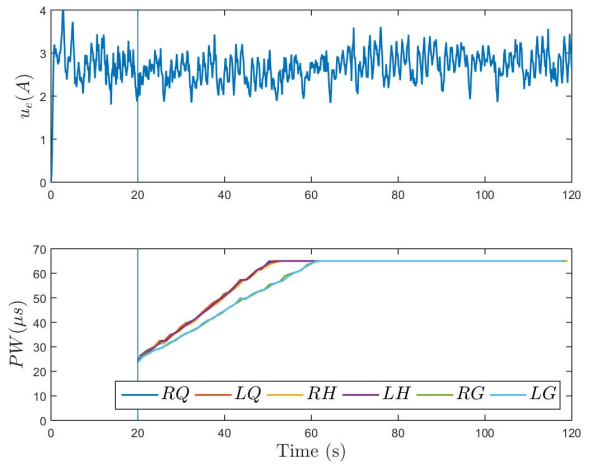

Fig. 5. P4B: (Top) Control effort sent to motor (Bottom) Control effort sent to rider's right (R) and left (L) quadriceps (Q), hamstring (H), and gluteal (G), respectively. Stimulation was saturated at 65 μs for rider comfort.

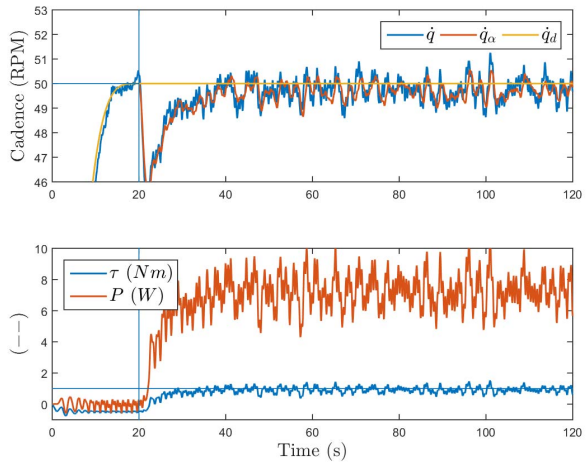

Fig. 6. P4D: (Top) Measured ($\dot{q}$), admitted ($\dot{q}_a$), and desired cadences ($\dot{q}_d$); (Bottom) Measured torque (τ) and estimated power (P) produced by the rider.

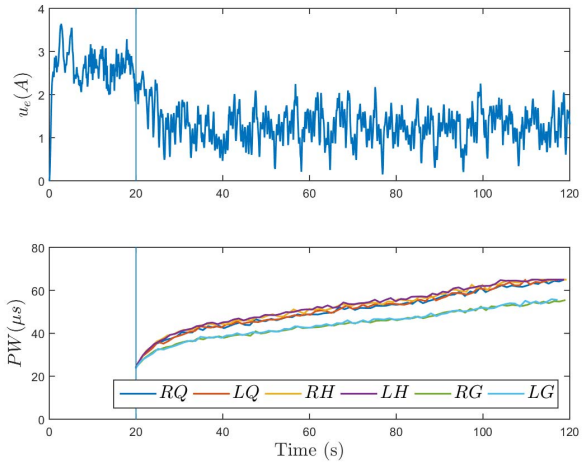

Fig. 7. P4D: (Top) Control effort sent to motor (Bottom) Control effort sent to rider's right (R) and left (L) quadriceps (Q), hamstring (H), and gluteal (G), respectively. Stimulation was saturated at 65 μs for rider comfort.

To testify to the admittance controller's capabilities to handle participant variability and ability, all participants were asked to repeat Protocol B, but with added volition (Protocol D). Figures 6 and 7 display the tracking results and control inputs for P4D, respectively. Compared to Figure 4, which displays P4's performance when he was asked to remain passive and not contribute to the pedaling task, Figure 6 shows notably improved tracking performance. When P4 was instructed to pedal, he not only was able to keep his stimulation levels below his saturation level, but also produce the desired torque (without modifying any gains). This trial more closely reflects the results displayed in Figures 2 and 3 for P3B. Meaning, if a participant is able to tolerate the required stimulation to produce the desired amount of torque, their performance will be similar to that as when they volitionally pedal (in the sense that they will be able to achieve the desired cadence at the desired torque). Therefore, the controller is capable of being applied to an individual with a complete spinal cord injury or an able-bodied individual that is volitionally pedaling, without any adjustment to the controller.

Figures 8 and 9 are provided to highlight the performance of P5, the participant with a spinal cord injury. Because she was unable to contribute volitionally to the cycling task, Protocol D was not completed. As illustrated in Figure 8, there was no improvement in the cadence tracking error over the course of the experiment. Correspondingly, this is attributed to the near-zero torque production elicited by the stimulation. It is hypothesized that because P5 experienced a spinal cord injury 12 years prior, her muscles had atrophied significantly and were small in comparison to other tissues present. According to [44], this can prevent the electricity from penetrating sufficiently deep into the leg to recruit muscle fibers for contraction. Consequently, despite reaching the maximum amount of stimulation deliverable by the stimulator (i.e., 500 μs) as shown in Figure 9, P5 is likely not receiving the full benefits of FES, but only of participating in range-of-motion exercises.

Despite P6 suffering a hemorrhagic stroke four years prior to her involvement in the study, she had regained some functional ability in the affected right arm and leg. Figure 10 displays the

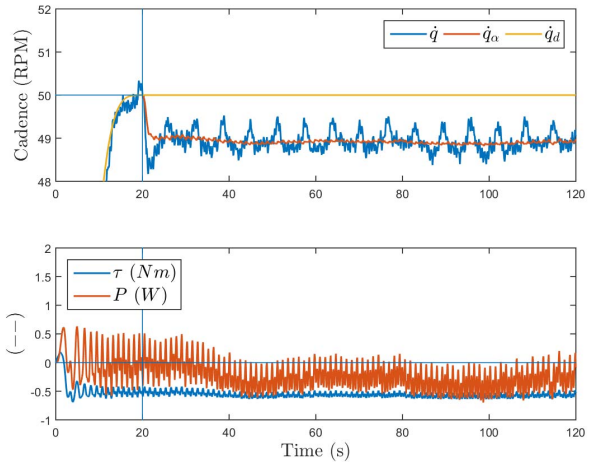

Fig. 8. P5C: (Top) Measured ($\dot{q}$), admitted ($\dot{q}_a$), and desired cadences ($\dot{q}_d$); (Bottom) Measured torque (τ) and estimated power (P) produced by the rider.

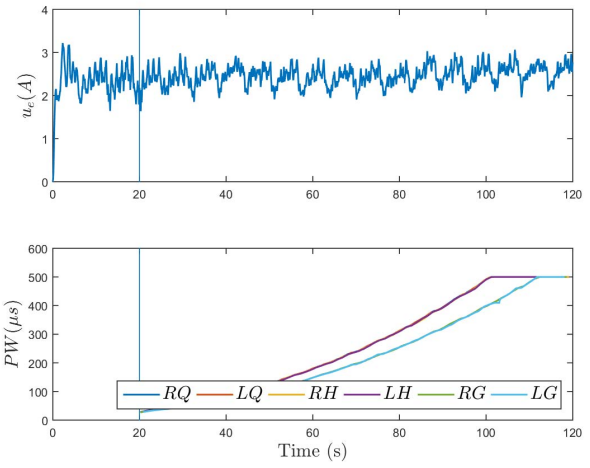

Fig. 9. P5C: (Top) Control effort sent to motor (Bottom) Control effort sent to rider's right (R) and left (L) quadriceps (Q), hamstring (H), and gluteal (G), respectively. Stimulation was saturated at 500 μs.

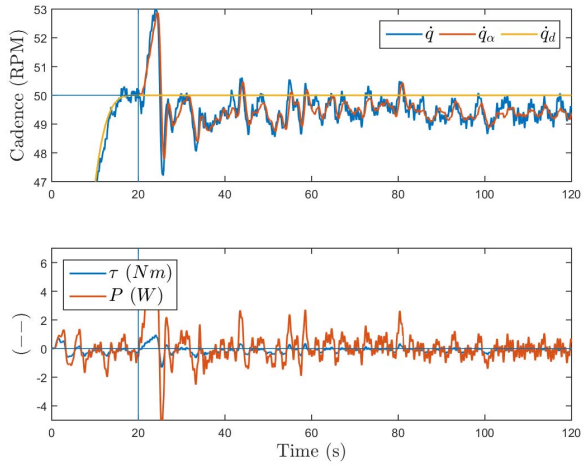

Fig. 10. P6D: (Top) Measured ($\dot{q}$), admitted ($\dot{q}_a$), and desired cadences ($\dot{q}_d$); (Bottom) Measured torque (τ) and estimated power (P) produced by the rider.

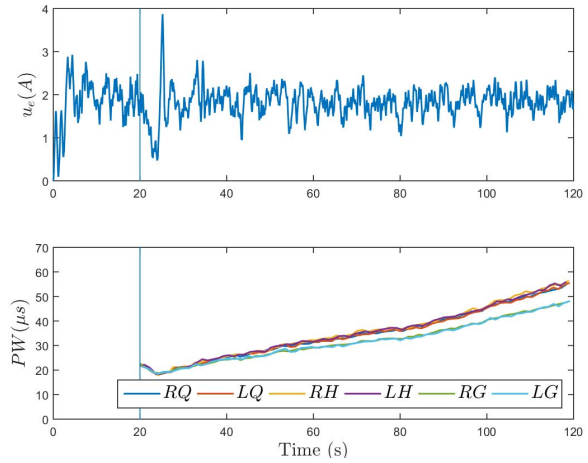

Fig. 11. P6D: (Top) Control effort sent to motor (Bottom) Control effort sent to rider's right (R) and left (L) quadriceps (Q), hamstring (H), and gluteal (G), respectively. Stimulation was saturated at 60 μs for rider comfort.

tracking results for P6D, when she was tasked with volitionally contributing to the cycling objective. Because P6 was able to pedal the cycle near the desired cadence, but with slight undershoot, she accumulated position and cadence error and correspondingly received an increasing amount of stimulation over the course of the experiment, as displayed in Figure 11. Because P6 was contributing volitionally, despite the increase in stimulation, she showed no sign of fatigue or decrease in torque production.

Although P7 had Parkinson's disease, he had ample muscle tone and strength due to his regular exercise regime. Accordingly, he was able to produce large amounts of torque and the desired interaction torque was varied according to Table II. When examining P7's trial with volition (P7D), it can be seen in Figure 12 that he is able to quickly track the desired cadence and meet the desired interaction torque. Compared to the counterpart protocol with the medium damping parameter (Protocol B), P7 was able to produce 44% more torque without significantly affecting the performance of the admittance controller. As depicted in Figure 13, P7 was able to keep his stimulation levels low by contributing volitionally. Furthermore, it can been seen that the rider is able to offset the current required by the motor to actuate the cycle.

Across all participants undergoing Protocols A-C, the low damping parameter selected for Protocol A resulted in the generation of the least-stiff admitted trajectory. The admitted trajectory was allowed to deviate the most, and consequently, the position/cadence errors were the largest across all protocols; this resulted in high stimulation and in the highest torque production. Comparatively, the highest damping parameter in Protocol C held the admitted trajectory close to the desired, reduced the position/cadence error, and resulted in the lowest torque production. Hence, without modifying the controller structure or gains, the FES cycle can place more or less emphasis on cadence tracking or torque production. Allowing riders to contribute volitionally (if possible) further increased

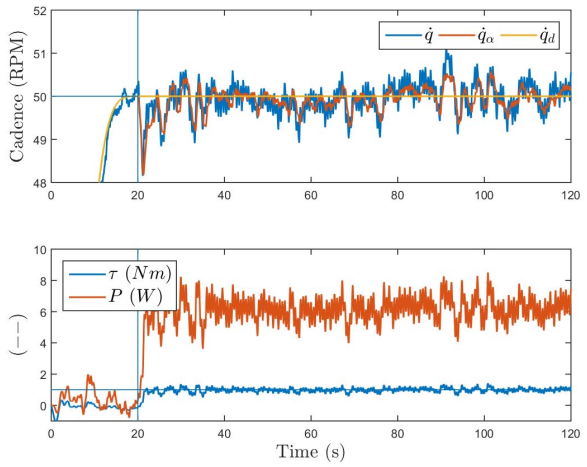

Fig. 12. P7D: (Top) Measured ($\dot{q}$), admitted ($\dot{q}_a$), and desired cadences ($\dot{q}_d$); (Bottom) Measured torque (τ) and estimated power (P) produced by the rider.

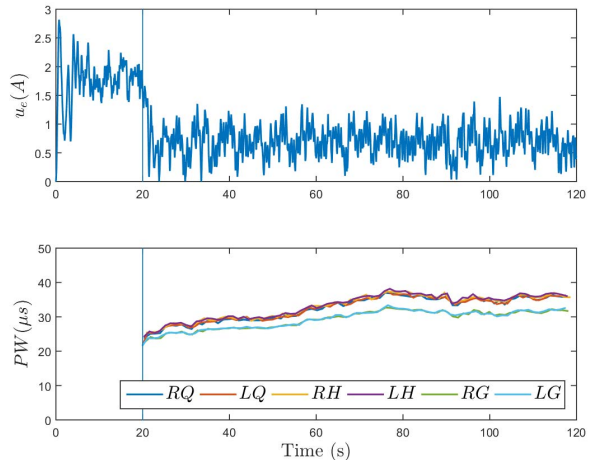

Fig. 13. P7D: (Top) Control effort sent to motor (Bottom) Control effort sent to rider's right (R) and left (L) quadriceps (Q), hamstring (H), and gluteal (G), respectively. Stimulation was saturated at 120 μs for rider comfort.

the torque production, especially when the desired interaction torque was set to a high value (e.g., 2.0 Nm). Accordingly, volition does not destabilize the controllers, nor compromise their performance, and should be encouraged whenever possible.

VI. Conclusion

FES cycling is a promising rehabilitation option for neurologically impaired individuals, and is an example of a hybrid rehabilitation robot which requires controllers to be implemented on both the human and the robot. By utilizing admittance control on the robot and guaranteeing passivity of the muscle stimulation controller through a Lyapunov-like stability analysis, safety is guaranteed in terms of the developed physical human-robot interaction. Experimental results are presented for three able-bodied participants and four participants with neurological conditions to demonstrate the efficacy of the proposed controllers. The admittance controller achieved an average admittance cadence error for Protocols A-C of -0.06 ± 1.47 RPM for able bodied participants and -0.02 ± 0.93 RPM for participants with NCs. The ease of use, comfort, and guaranteed safety makes this FES cycle a promising method for future rehabilitation strategies, particularly in terms of in-home use.

Acknowledgment

Any opinions, findings and conclusions, or recommendations expressed in this material are those of the author(s) and do not necessarily reflect the views of the sponsoring agency.

References

[1] E. J. Benjamin *et al.*, "Heart disease and stroke statistics-2017 update: A report from the american heart association," *Circulation*, vol. 135, no. 10, pp. e146–e603, 2017.

[2] F. Anaya, P. Thangavel, and H. Yu, "Hybrid FES—Robotic gait rehabilitation technologies: A review on mechanical design, actuation, and control strategies," *Int. J. Intell. Robot. Appl.*, vol. 2, no. 1, pp. 1–28, Mar. 2018.

[3] M. Bélanger, R. B. Stein, G. D. Wheeler, T. Gordon, and B. Leduc, "Electrical stimulation: Can it increase muscle strength and reverse osteopenia in spinal cord injured individuals?" *Arch. Phys. Med. Rehabil.*, vol. 81, no. 8, pp. 1090–1098, Aug. 2000.

[4] T. Mohr, J. Pødenphant, F. B.-Sørensen, H. Galbo, G. Thamsborg, and M. Kjær, "Increased bone mineral density after prolonged electrically induced cycle training of paralyzed limbs in spinal cord injured man," *Calcified Tissue Int.*, vol. 61, no. 1, pp. 22–25, 1997.

[5] H. I. Krebs and B. T. Volpe, "Robotics: A rehabilitation modality," *Current Phys. Med. Rehabil. Rep.*, vol. 3, no. 4, pp. 243–247, 2015.

[6] L. J. Marchal-Crespo and D. J. Reinkensmeyer, "Review of control strategies for robotic movement training after neurologic injury," *J. Neuroeng. Rehabil.*, vol. 6, p. 20, Dec. 2009.

[7] C. Ott, R. Mukherjee, and Y. Nakamura, "Unified impedance and admittance control," in *Proc. IEEE Int. Conf. Robot. Automat.*, May 2010, pp. 554–561.

[8] P. K. Jamwal, S. Hussain, M. H. Ghayesh, and S. V. Rogozina, "Impedance control of an intrinsically compliant parallel ankle rehabilitation robot," *IEEE Trans. Ind. Electron.*, vol. 63, no. 6, pp. 3638–3647, Jun. 2016.

[9] N. Hogan, "Impedance control-an approach to manipulation.I-Theory.II-implementation.III -applications," *J. Dyn. Syst. Meas. Control*, vol. 107, no. 1, pp. 1–24, Jan. 1985.

[10] H. Lee and N. Hogan, "Essential considerations for design and control of human-interactive robots," in *Proc. IEEE Int. Conf. Robot. Automat.*, May 2016, pp. 3069–3074.

[11] I. Ranatunga, F. L. Lewis, D. O. Popa, and S. M. Tousif, "Adaptive admittance control for human–robot interaction using model reference design and adaptive inverse filtering," *IEEE Trans. Control Syst. Technol.*, vol. 25, no. 1, pp. 278–285, Jan. 2017.

[12] M. J. Bellman, R. J. Downey, A. Parikh, and W. E. Dixon, "Automatic control of cycling induced by functional electrical stimulation with electric motor assistance," *IEEE Trans. Automat. Sci. Eng.*, vol. 14, no. 2, pp. 1225–1234, Apr. 2017.

[13] A. J. van Soest, M. Gföhler, and L. J. Casius, "Consequences of ankle joint fixation on FES cycling power output: A simulation study," *Med. Sci. Sports Exerc.*, vol. 37, no. 5, pp. 797–806, 2005.

[14] C. Fornusek and G. M. Davis, "Maximizing muscle force via low-cadence functional electrical stimulation cycling," *J. Rehabil. Med.*, vol. 36, no. 5, pp. 232–237, 2004.

[15] J. Szecsi, A. Straube, and C. Fornusek, "Comparison of the pedalling performance induced by magnetic and electrical stimulation cycle ergometry in able-bodied subjects," *Med. Eng. Phys.*, vol. 36, no. 4, pp. 484–489, Apr. 2014.

[16] D. J. Newham and N. de N. Donaldson, "FES cycling," *J. Autom. Control*, vol. 18, no. 2, pp. 73–76, 2008.

[17] L. D. Duffell *et al.*, "Long-term intensive electrically stimulated cycling by spinal cord–injured people: Effect on muscle properties and their relation to power output," *Muscle Nerve*, vol. 38, no. 4, pp. 1304–1311, 2008.

[18] C. A. Coste and P. Wolf, "FES-cycling at cybathlon 2016: Overview on teams and results," *Artif. Organs*, vol. 42, no. 3, pp. 336–341, 2018.

[19] E. Ambrosini, S. Ferrante, G. Ferrigno, F. Molteni, and A. Pedrocchi, "Cycling induced by electrical stimulation improves muscle activation and symmetry during pedaling in hemiparetic patients," *IEEE Trans. Neural Syst. Rehabil. Eng.*, vol. 20, no. 3, pp. 320–330, May 2012.

[20] K. J. Hunt *et al.*, "Control strategies for integration of electric motor assist and functional electrical stimulation in paraplegic cycling: Utility for exercise testing and mobile cycling," *IEEE Trans. Neural Syst. Rehabil. Eng.*, vol. 12, no. 1, pp. 89–101, Mar. 2004.

[21] A. Farhoud and A. Erfanian, "Fully automatic control of paraplegic FES pedaling using higher-order sliding mode and fuzzy logic control," *IEEE Trans. Neural Syst. Rehabil. Eng.*, vol. 22, no. 3, pp. 533–542, May 2014.

[22] D. Liberzon, *Switching in Systems and Control*. Basel, Switzerland: Birkhauser, 2003.

[23] G. Herrnstadt and C. Menon, "Admittance-based voluntary-driven motion with speed-controlled tremor rejection," *IEEE/ASME Trans. Mechatron.*, vol. 21, no. 4, pp. 2108–2119, Aug. 2016.

[24] Q. Wu, X. Wang, B. Chen, and H. Wu, "Development of a minimal-intervention-based admittance control strategy for upper extremity rehabilitation exoskeleton," *IEEE Trans. Syst., Man, Cybern., Syst.*, vol. 46, no. 6, pp. 1005–1016, Jun. 2018.

[25] V. H. Duenas, C. A. Cousin, A. Parikh, P. Freeborn, E. J. Fox, and W. E. Dixon, "Motorized and functional electrical stimulation induced cycling via switched repetitive learning control," *IEEE Trans. Control Syst. Technol.*, to be published.

[26] V. H. Duenas, C. Cousin, V. Ghanbari, and W. E. Dixon, "Passivity-based learning control for torque and cadence tracking in functional electrical stimulation (FES) induced cycling," in *Proc. Annu. Amer. Control Conf. (ACC)*, Jun. 2018, pp. 3726–3731.

[27] C. A. Cousin, V. H. Duenas, C. A. Rouse, and W. E. Dixon, "Stable cadence tracking of admitting functional electrical stimulation cycle," in *Proc. ASME Dyn. Syst. Control Conf.*, Sep. 2018, Art. no. V001T07A003.

[28] C. A. Cousin, V. Duenas, C. A. Rouse, and W. E. Dixon, "Admittance control of motorized functional electrical stimulation cycle," *IFAC-Papers OnLine*, vol. 51, no. 34, pp. 272–277, 2019.

[29] C. A. Cousin, V. H. Duenas, C. A. Rouse, and W. E. Dixon, "Cadence and admittance control of a motorized functional electrical stimulation cycle," in *Proc. IEEE Conf. Decis. Control*, Dec. 2018, pp. 6470–6475.

[30] D. B. Popović, "Advances in functional electrical stimulation (FES)," *Journal Electromyograph. Kinesiol.*, vol. 24, no. 6, pp. 795–802, Dec. 2014.

[31] M. Ferrarin, F. Palazzo, R. Riener, and J. Quintern, "Model-based control of FES-induced single joint movements," *IEEE Trans. Neural Syst. Rehabil. Eng.*, vol. 9, no. 3, pp. 245–257, Sep. 2001.

[32] N. Sharma, K. Stegath, C. M. Gregory, and E. W. Dixon, "Nonlinear neuromuscular electrical stimulation tracking control of a human limb," *IEEE Trans. Neural Syst. Rehabil. Eng.*, vol. 17, no. 6, pp. 576–584, Dec. 2009.

[33] K. P. Tee, R. Yan, and H. Li, "Adaptive admittance control of a robot manipulator under task space constraint," in *Proc. IEEE Int. Conf. Robot. Autom.*, May 2010, pp. 5181–5186.

[34] Y. Li and S. S. Ge, "Impedance learning for robots interacting with unknown environments," *IEEE Trans. Control Syst. Technol.*, vol. 22, no. 4, pp. 1422–1432, Jul. 2014.

[35] H. K. Khalil, *Nonlinear Systems*, 3rd ed. Upper Saddle River, NJ, USA: Prentice-Hall, 2002.

[36] A. F. Filippov, "Differential equations with discontinuous righthand sides," in *Fifteen Papers on Differential Equations* (American Mathematical Society Translations), vol. 42. Providence, RI, USA: American Mathematical Society, 1964, pp. 199–231.

[37] B. E. Paden and S. S. Sastry, "A calculus for computing Filippov's differential inclusion with application to the variable structure control of robot manipulators," in *Proc. 25th IEEE Conf. Decis. Control*, Dec. 1986, pp. 578–582.

[38] C. A. Rouse, C. A. Cousin, V. H. Duenas, and W. E. Dixon, "Cadence tracking for switched FES cycling combined with voluntary pedaling and motor resistance," in *Proc. Annu. Amer. Control Conf.*, Jun. 2018, pp. 4558–4563.

[39] N. Stefanovic, M. Ding, and L. Pavel, "An application of L_2 nonlinear control and gain scheduling to erbium doped fiber amplifiers," *Control Eng. Pract.*, vol. 15, no. 9, pp. 1107–1117, 2007.

[40] T. Fujinaka, Y. Kishida, M. Yoshioka, and S. Omatu, "Stabilization of double inverted pendulum with self-tuning neuro-PID," in *Proc. IEEE-INNS-ENNS Int. Joint Conf. Neural Netw.*, Jul. 2000, pp. 345–348.

[41] F. Nagata, K. Kuribayashi, K. Kiguchi, and K. Watanabe, "Simulation of fine gain tuning using genetic algorithms for model-based robotic servo controllers," in *Proc. Int. Symp. Comput. Intell. Robot. Automat.*, Jun. 2007, pp. 196–201.

[42] N. J. Killingsworth and M. Krstic, "PID tuning using extremum seeking: Online, model-free performance optimization," *IEEE Control Syst. Mag.*, vol. 26, no. 1, pp. 70–79, Feb. 2006.

[43] R. Kelly, V. Santibanez, and A. Loria, *Control Robot Manipulators Joint Space*. Berlin, Germany: Springer Science and Business Media, 2005.

[44] M. Laubacher *et al.*, "Stimulation of paralysed quadriceps muscles with sequentially and spatially distributed electrodes during dynamic knee extension," *J. Neuroeng. Rehabil.*, vol. 16, no. 1, p. 5, 2019.